Cell. Mol. Life Sci. (2014) 71:3811–3828
DOI 10.1007/s00018-014-1577-4

Cellular and Molecular Life Sciences

RESEARCH ARTICLE

Fibulin-2 is involved in early extracellular matrix development of the outgrowing mouse mammary epithelium

D. Olijnyk · A. M. Ibrahim · R. K. Ferrier · T. Tsuda · M.-L. Chu · B. A. Gusterson · T. Stein · J. S. Morris

Received: 4 October 2013 / Accepted: 27 January 2014 / Published online: 13 February 2014

Abstract Cell–matrix interactions control outgrowth of mammary epithelium during puberty and pregnancy. We demonstrate here that the glycoprotein fibulin-2 (FBLN2) is strongly associated with pubertal and early pregnant mouse mammary epithelial outgrowth. FBLN2 was specifically localized to the cap cells of the terminal end buds during puberty and to myoepithelial cells during very early pregnancy (days 2–3) even before morphological changes to the epithelium become microscopically visible, but was down-regulated thereafter. Exposure to exogenous oestrogen (E2) or E2 plus progesterone (P) increased *Fbln2* mRNA expression in the pubertal gland, indicating hormonal control. FBLN2 was co-expressed and co-localised with the proteoglycan versican (VCAN) and co-localised with laminin (LN), while over-expression of FBLN2 in HC-11 cells increased cell adhesion to several extracellular matrix proteins including LN and fibronectin, but not collagens. Mammary glands from *Fbln2* knockout mice showed no obvious phenotype but increased fibulin-1 (FBLN1) staining was detected, suggesting a compensatory mechanism by other fibulin family members. We hypothesise that similar to embryonic aortic smooth muscle development, FBLN2 and VCAN expression alters the cell–matrix interaction to allow mammary ductal outgrowth and development during puberty and to enable epithelial budding during pregnancy.

Keywords Terminal end buds · Mammary gland · Fibulin-2 · Versican · Epithelial-stromal interactions

Abbreviations

BM	Basement membrane
CMV	Cytomegalovirus
Ctrl	Control
DAPI	4′,6-diamidino-2-phenylindole
DMEM	Dulbecco's Modified Eagle's Medium
ECM	Extracellular matrix
E2	Estradiol
EGF	Epidermal growth factor
ER	Oestrogen receptor
FBS	Foetal bovine serum
FFPE	Formalin-fixed paraffin-embedded
FN	Fibronectin

T. Stein and J.S. Morris contributed equally to this project.

Electronic supplementary material The online version of this article (doi:10.1007/s00018-014-1577-4) contains supplementary material, which is available to authorized users.

D. Olijnyk · A. M. Ibrahim · B. A. Gusterson · T. Stein (✉)
Institute of Cancer Sciences, College of MVLS, University of Glasgow, Glasgow G12 8QQ, UK
e-mail: Torsten.Stein@glasgow.ac.uk

A. M. Ibrahim
Zoology Department, Faculty of Science, Cairo University, Giza 12613, Egypt

R. K. Ferrier
MVLS Pathology Unit Pathology Department, Southern General Hospital, Glasgow G51 4TF, UK

T. Tsuda
Nemours Biomedical Research and Nemours Cardiac Center, Alfred I. duPont Hospital for Children, Wilmington 19803, USA

M.-L. Chu
Department of Dermatology and Cutaneous Biology, Thomas Jefferson University, Philadelphia, PA 19107, USA

J. S. Morris (✉)
School of Veterinary Medicine, College of MVLS, University of Glasgow, Bearsden Road, Glasgow G61 1QH, UK
e-mail: Joanna.Morris@glasgow.ac.uk

Fwd	Forward
HRP	Horseradish peroxidase
IF	Immunofluorescence
IgG	Immunoglobulin G
IHC	Immunohistochemistry
KO	Knock-out
Krt	Cytokeratin
LN111	Laminin-111
LN332	Laminin-332
LTBP1	Latent TGFβ binding protein 1
P	Progesterone
Post-LN	Post-lymph node (area beyond major mammary lymph node)
Pre-LN	Pre-lymph node (area between nipple and major mammary lymph node)
qRT-PCR	Quantitative reverse transcriptase polymerase chain reaction
rev	Reverse
RGD	Argine, glycine, aspartate
RIPA	Radio immunoprecipitation assay
RPMI	Roswell Park Memorial Institute
SD	Standard deviation
SEM	Standard error of the mean
TEB	Terminal end bud
TGFβ	Transforming growth factor beta
VCAN	Versican

Introduction

Cell–matrix interactions are key regulators of mammary gland development [1]. The mammary gland comprises inner luminal and outer myoepithelial cell layers, surrounded by an extracellular matrix (ECM) consisting of basal lamina proteoglycans and glycoproteins (basement membrane; BM), and fibrous connective tissue, including fibrillar collagens, elastic fibres, and fibronectin (FN). The myoepithelium directly contacts the BM through integrins and transmembrane proteoglycans, and these interactions are vital for development of the mammary epithelial network and cell fate.

At puberty, the mouse mammary epithelium expands and invades the surrounding mammary fat pad to form the primary ductal network. Around three weeks of age, in response to hormonal changes, the epithelial tree elongates dramatically and branches to fill the mammary fat pad. This process is driven by highly specialised, proliferative structures at the duct ends, which are the terminal end buds (TEB) [2]. Similarly, during each pregnancy cycle these ducts bud and form secretory alveoli, which later regress after lactation to form a mammary epithelium that resembles a pre-pregnancy state. These changes require high flexibility and remodelling of the surrounding ECM [1, 3].

Originally isolated from fibroblasts [4] and identified as components of connective tissue elastic fibres [5], fibulins have since been found to play much wider roles in tissue development [6]. Fibulins are a highly conserved family of ECM glycoproteins, which in mammals consists of eight members. All fibulins contain a series of epidermal growth factor (EGF)-like motifs, and a carboxy-terminal fibulin-type module (FC domain), while their N-termini are highly variable in size and modular structure [7]. Within the protein family, fibulin-1 (FBLN1) and -2 are most similar to each other as they both contain three anaphylatoxin-like motifs not present in other fibulins. However, fibulin-2 (FBLN2) is much larger than FBLN1 owing to the presence of a unique N-terminal domain of ~400 amino acids, which consists of cysteine rich (Na) and cysteine free (Nb) subdomains. Sequence prediction of mouse FBLN2 indicates four potential N-linked glycosylation sites and a single Arg-Gly-Asp (RGD) attachment site, indicative of adhesive properties. Alternative splicing of *Fbln2* produces two variants, V1 (18 exons) and V2 (17 exons) with V2 lacking EGF-like domain 3 (aa709–755), encoded by exon 9.

In vitro studies indicate that fibulins interact with a range of ECM proteins and thereby link and stabilize the organisation of supramolecular ECM structures, including basement membranes, elastic fibres and fibronectin matrix [8–10]. FBLN2 interacts with fibrillin-1 (FBN1) in microfibril bundles that intersect the lamina densa of kidney glomeruli and the dermal-epidermal junction [11]. However, the timing of its expression and spatial localisation within the tissues also suggest that it may promote either proliferation or differentiation or migration of mesenchymal cells during organogenesis and endorse structural stability during adulthood. FBLN2 may also have a functional role in the female and male reproduction systems since it is expressed in testis [12] and ovaries [13] and can sequester sex hormone binding globulin (SHBG) within the stroma of the uterus, thus regulating the access of SHBG to target cells [14]. Finally, since it is over-expressed during wound repair processes, FBLN2 may also influence tissue remodelling [15, 16].

The role of FBLN2 in organogenesis, tissue remodelling, cell adhesion and migration in different biological systems identified this gene as a candidate for regulating mouse mammary gland morphogenesis. In this study, we aimed to examine the FBLN2 expression pattern during normal mouse mammary gland development, with a focus on puberty. We also examined the expression patterns of its binding partners, the influence of systemic hormones on its expression in vivo and its role in the regulation of cell migration and adhesion in vitro. Finally, we investigated the role of FBLN2 in pubertal morphogenesis by examining ductal tree morphology in *Fbln2* KO mice. We show for the first time that FBLN2's expression pattern and localisation

make it a potential novel regulator of mammary epithelial outgrowth, and that FBLN1 up-regulation compensates for loss of FBLN2 in the pubertal gland.

Methods

Animal husbandry and treatment

All animals were kept according to UK Home Office guidelines and the project was approved by the University of Glasgow ethics committee. Six-week-old C57BL/6 mice were purchased from Harlan Laboratories UK. C57BL/6 mice with CAG promoter-driven EGFP expression [17] were a kind gift from Prof. Brisken (EPFL/ISREC, Lausanne, Switzerland). *Fbln2* KO mice have been described previously [18].

Hormonal treatment (priming) was administered to 3.5 week old female mice using subcutaneous pellets (Innovative Research of America, USA), which delivered standardized, continuous release of the active ingredient over a given period of time: 21 day release oestrogen (E2) (0.72 mg/pellet), oestrogen-progesterone (E2+P) (0.1 mg/pellet, 10 mg/pellet) or placebo (10.01 mg/pellet). Pellet implantation was performed on anaesthetised mice in a pocket created under the skin at the back of the neck. Implanted mice were primed with hormones for seven days, then culled to collect the mammary glands.

Whole mount preparation

After dissection, the fourth inguinal mammary glands were spread on microscope slides, fixed in Carnoy's fixative for 3 h at room temperature (RT), hydrated through decreasing concentrations of ethanol followed by distilled water, and stained overnight with Carmine dye. The gland was then dehydrated through serially increasing concentrations of ethanol followed by xylene, coverslipped and stored at RT.

Collection of isolated epithelium (TEB and ducts)

For each isolation, 20 inguinal glands from 6 to 8 week old wild-type C57BL/6 mice were removed, coarsely minced and digested with 1 mg/ml (w/v) collagenase type II (Sigma, Aldrich Company Ltd., Dorset, UK) in Leibovitz L-15 medium (Invitrogen, Life Technologies, Paisley, UK) for 35 min as described previously [19]. The released TEB and ducts were visualised by means of a dissecting microscope (Olympus Ltd., Surrey, UK) and manually collected using a Gilson pipette into 50–100 µl of Trizol Reagent (Invitrogen) and stored at −80 °C prior to extraction of RNA. There were 1,145 TEB and 1,111 ducts collected from ~300 mice.

Collection of mouse mammary gland tissue strips

Inguinal mammary glands from 7 week old heterozygous EGFP expressing C57BL/6 littermates were excised, gently spread onto glass slides and visualised using a Stemi V6 fluorescent dissecting microscope (Carl Zeiss Ltd., Cambridge, UK). Tissue strips corresponding to pre-lymph node (Pre-LN), post-lymph node (Post-LN) and empty fat pad (Fat pad) were cut using sterile scalpel blades, snap frozen and stored at −80 °C, as described previously [19].

RNA isolation from frozen tissue and isolated epithelium

Extraction of RNA from frozen tissue and epithelial samples in Trizol Reagent (Invitrogen) was performed according to the manufacturer's instructions and as described previously [19, 20]. TEB from individual enzymatic dissections were pooled together in a final volume of 1 ml of Trizol Reagent prior to extraction, as were all ducts. After extraction, all RNA isolated from TEB ($n = 1{,}145$) was combined, as was all RNA obtained from ducts ($n = 1{,}111$). On-column purification was used to remove small RNA fragments (RNeasy Micro Kit, Qiagen, Crawley, UK). RNA was quantified using the NanodropND-1000 Spectrophotometer (Thermo Fisher Scientific, Rockford, IL, USA) and its quality assessed using an Agilent bioanalyser (Agilent Technologies, Santa Clara, CA, USA).

qRT PCR

The cDNA was produced from DNase I treated RNA using SuperscriptII (Invitrogen). A negative control lacking reverse transcriptase (-RT) was used in all reaction runs. There was 1 µl of template cDNA used in each PCR reaction with FastStart Taq DNA Polymerase (Roche, Burgess Hill, UK) in a final reaction volume of 20 µl. PCR was carried out using a LightCycler® 480 Instrument (Roche) under standard conditions. Primers: *Fbln2*: V1 Fwd 5′-tgttgttggggacacagcta-3′, Rev 5′-ccatcaaacactcgtcttggt-3′; *Fbln2*: Fwd 5′-tctgtccccagaggtgatct-3′, Rev 5′-ctgcacaacaggtctcgattag-3′; *Sprr1A*: Fwd 5′-cctgaagacctgatcaccaga-3′, Rev 5′-aggcaatgggactcataagc-3′; *Ltf*: Fwd 5′-gggcaagtgcggtttagtt-3′, Rev 5′-ccattgcttttggaggattt-3′; *Vcan*: Fwd 5′-cactggctgtggatggtg-3′, Rev- 5′-cagcggcaaagttcagagt-3′ and *Krt18*: Fwd 5′-agatgacaccaacatcacaag-3′, Rev 5′-cttccagaccttggacttcct-3′ (all Sigma). Relative RNA expression was calculated by the $2^{-\Delta\Delta Cp}$ method.

PCR

PCR reactions were prepared using GoTaq® DNA Polymerase (Promega UK, Southampton, UK) according to manufacturer's recommendations, using between 28

and 30 cycles. Primers: mouse *Fbln2* V1: Fwd 5′-cctgcaaagacaatggaccc-3′, Rev 5′-tcgtccacgtctgtgcattc-3′; mouse *Fbln2* V2: Fwd 5′-cctgcaaagacaatggaccc-3′, Rev 5′-tcgtccacgtctgtgcattc-3′.

PCR products were separated by 1.5 % agarose gel electrophoresis stained with ethidium bromide together with a 100 bp DNA ladder as a size marker. Gels were examined using Fujifilm Fla-5000 and FLA5000 Image Reader software v. 2.0 (Fujifilm UK Ltd., Sheffield, UK). Images were manipulated using an Advanced Image Data Analyser v. 4.13 (Aida) (Fujifilm UK Ltd.) or Adobe Photoshop CS2 (Adobe Photoshop Systems Inc., Mountain View, US).

Cell culture

All cells were grown under sterile conditions at 37 °C in a humidified atmosphere and 5 % CO_2 with specific requirements as follows: EpH4 cells—Dulbecco's Modified Eagle's Medium (DMEM), 10 % FBS, 2 mM L-glutamine; HC-11 cells—RPMI-1,640, 10 % FBS, 2 mM L-glutamine, 5 μl/ml insulin, 10 ng/ml EGF and NIH3T3 cells—DMEM, 10 % FBS, 2 mM L-glutamine (all Invitrogen).

Plasmid purification

The pRc/CMV-*Fbln2* containing variant 1 (V1) of the mouse *Fbln2* gene (NM_007992) under the control of a Cytomegalovirus (CMV) promoter was used to express FBLN2 in cells with an empty vector pcDNA3 (98 % sequence identity to pRc/CMV) as a negative transfection control. Plasmid DNA was purified using the QIAprep Miniprep kit and HiSpeed® Plasmid Maxi (Qiagen) as per manufacturer's instructions. The DNA was quantified using a NanoDrop ND-1000 Spectrophotometer.

Transfection

Logarithmically growing HC-11 cells were transfected with 4 μg pRc/CMV-*Fbln2* with Lipofectamine™ transfection reagent (Invitrogen) using a 1:1 ratio in reduced serum medium according to manufacturer's instructions and incubated at 37 °C for 5 h before changing the culture medium and further incubation for 48 h. Transfected HC-11 cells were then incubated for 48 h prior to being collected in radio immunoprecipitation assay (RIPA) buffer for protein extraction or used for further applications.

Migration assay

HC-11 cells were transfected in triplicate for 48 h. A double cross was marked on the surface of each well of confluent cells using a sterile 200 μl pipette tip. Culture medium was collected from each well, spun down at RT for 5 min at 1,100 rcf to discard floating cells, mixed with fresh culture medium and placed back on the cells. For each well two areas around the double cross were imaged at 0, 4, 7, 11, 24 and 36 h. Image analysis was performed using an Olympus IX51 inverted microscope (Olympus) with F-view Soft Imaging System and Cell^{P} Imaging software (Olympus). The gap width was measured in triplicate for each selected area at 400× magnification and the experiment was repeated thrice. Cells were finally collected for protein extraction to determine transgene expression.

Adhesion assay

The adhesiveness of *Fbln2* transfected HC-11 cells to wells coated with seven human ECM proteins or with BSA as a negative control was studied using a 96-well ECM Cell Adhesion Array Kit (Chemicon/Merck Millipore, Billerica, MA, USA) with colorimetric detection according to manufacturer's instruction. Briefly, HC-11 cells were transfected for 48 h with either pRc/CMV-*Fbln2* or empty vector control (pcDNA3), before cells were detached from the plastic by incubation in 2 mM EDTA/PBS solution for 20 min. Expression of FBLN2 was verified by western blotting. The transfected cells were then plated in triplicate in 96-well cell culture plates precoated with ECM proteins using 1.5×10^6 cells/ml. Cells were left to adhere for 2 h in a 5 % CO_2 incubator at 37 °C before removal of non-adhered cells, followed by staining and lysis of the adhered cells. Staining intensity was measured with a microplate reader at 570 nm. The relative cell attachment was determined as compared to the negative control (BSA).

Protein extraction

Cells were washed twice with dPBS and incubated on ice with ice cold RIPA lysis buffer with protease inhibitor cocktail (Roche) for 15 min with occasional mixing, centrifuged at 4 °C for 20 min at 25,000 rcf and the supernatant protein quantified with the BCA™ Protein Assay Kit (Pierce, Thermo Fisher Scientific) according to the manufacturer's instructions. For frozen tissues, samples were pooled or individually crushed in liquid nitrogen using a mortar and pestle cooled on dry ice, then transferred to a Down's Homogeniser chilled on dry ice and resuspended in 0.5 ml of ice cold RIPA lysis buffer with protease inhibitors. Homogenised samples were transferred to ice chilled 1.5 ml microcentrifuge tubes and frozen on dry ice. Tissue lysates were then defrosted, incubated on ice for 30 min to facilitate further cell lysis and centrifuged at 25,000 rcf at 4 °C for 20 min. The resulting supernatant was retained, quantified, and concentrated as necessary using a Microcon® Centrifugal Filter Device with Ultracel YM-3 membrane (Ambion, Life Technologies).

Electrophoresis and Western blotting

The 25–50 μg protein extracts were separated using either 4–12 % Bis–Tris Novex NuPage™ gels (Invitrogen) or 3–8 % Tris–Acetate polyacrylamide gels according to manufacturer's instructions. Novex® Sharp Pre-stained Protein Standards were separated alongside the samples. Seperated proteins were transferred onto Whatman® Protran® Nitrocellulose Transfer Membrane (0.2 μm) (GE Healthcare UK Ltd., Chalfont St Giles, UK) using a Novex XCell II™ Blot module (Invitrogen). Ponceau S staining was used to determine the efficiency of the transfer. The blotted membrane was blocked with 4 % dried skimmed milk blocking solution (TBS, 0.1 % Tween-20), then incubated for 2 h at RT or overnight at 4 °C with primary antibody followed by incubation for 1 h at RT with the appropriate horseradish peroxidase (HRP)-conjugated secondary antibody. Final working concentrations: rabbit polyclonal anti-FBLN2 [21], 1:5,000; goat polyclonal anti-actin (C20, Santa Cruz, USA) 1:1,000; HRP-conjugated polyclonal rabbit anti-goat IgG (Dako UK Ltd, Ely, UK) 1:3,000; and HRP-conjugated polyclonal donkey anti-rabbit IgG-HRP labelled (GE Healthcare UK Ltd.) 1:5,000. Signal detection was performed using the ECL Western blotting detection reagents (Pierce) as per manufacturer's instructions and an Intelligent Dark Box LAS-3000 equipped with a cooled to −30 °C charge coupled device, camera and FO.85 Fujinon Lens. Images were acquired and analysed using LAS-3000 v.2.2 software (Fujifilm UK Ltd.) after 4–20 min of exposure under standard sensitivity.

Immunohistochemistry and immunofluorescence

The 3–4 μm sections were routinely cut from formalin-fixed, paraffin wax embedded mammary glands (10 μm sections for 3D structure reconstruction experiments). Antigen retrieval was performed using 1 mM EDTA buffer (pH 8) under high pressure and all other incubations were performed at RT using a humidity chamber. Sections were blocked with pre-diluted 2.5 % horse serum for 20 min then incubated with primary antibody for 30 min. All antibodies were diluted to their final concentrations using Antibody Diluent (DAKO UK Ltd.) (rabbit polyclonal anti-FBLN2 1:10,000 [21]; rabbit polyclonal anti-FBLN1 1:1,000 [22]; rabbit polyclonal anti-VCAN 1:100 (ab1033, Millipore/Chemicon, Billerica, USA), 1:100 rabbit polyclonal anti-Laminin-111 (L9393, Sigma). Washed tissue sections were incubated for 30 min with Donkey polyclonal anti-rabbit (HRP labelled) secondary antibody diluted 1:500, prior to staining with DAB + Chromogen for 4 min. Stained tissue sections were counterstained with haematoxylin, dehydrated through increasing concentrations of ethanol then xylene before mounting with cover slips using Pertex mounting medium (CellPath, Newtown, Powys, UK). Negative control (lacking primary antibody) and positive control (tissue known to express protein of interest) were used in each staining run. Tissue sections were examined using a Labophot-2 light microscope and imaged and scanned using a NanoZoomer Digital Pathology scanner at 20× magnification. The obtained images were then manipulated and analysed using Digital Image Hub (Leica Biosystems UK Ltd, Milton Keynes, UK) and staining semi-quantified using the quickscore method [23], in which the overall quickscore is defined as the percentage score (1: 0–4 %, 2:5–19 %, 3: 20–39 %, 4: 40–59 %, 5: 60–79 %, 6: >79 %) multiplied with an intensity score (0: negative, 1: weak, 2: intermediate, 3: strong), giving a final value between 0 (not expressed) and 18 (strong expression in 100 % of target tissue).

For IF, tissue sections were blocked with Image-iT™ FX Signal Enhancer (Invitrogen) for 30 min before incubation in 2.5 % Horse Serum. Primary antibodies were used at: rabbit polyclonal anti-FBLN2 [21] 1:15,000; and rabbit polyclonal anti-FN (ab2413, Abcam Inc, Cambridge, MA, USA) 1:1,000. Alexa Fluor conjugated secondary antibodies (Alexa Fluor 488; Alexa Fluor 594, Invitrogen) were used at 1:1,000 dilution and incubated for 20 min in darkness. Tissue sections were mounted using ProLong® Gold antifade reagent with DAPI (Invitrogen). Tissue sections were imaged using a Leica TCS SP2 confocal microscope with 63× oil immersion lens and Leica Confocal Software (Leica Biosystems UK Ltd.).

Results

Fbln2 mRNA and protein is expressed during epithelial growth initiation and primary expansion

To assess whether FBLN2 was associated with distinct stages of mammary gland development, we measured *Fbln2* mRNA levels across puberty, pregnancy, lactation and involution by qRT PCR (Fig. 1a). Expression levels were normalised to *Krt18* mRNA expression to adjust for changes in epithelial expansion. The highest mRNA abundance was found in mammary glands of pubertal and early pregnant mice after which it was steadily reduced. *Fbln2* mRNA was, therefore, most abundant during pubertal epithelial primary outgrowth and when the epithelial network starts to expand further during pregnancy. However, when normalized to *Krt14* the strongest expression was only found during puberty (Supplementary Figure 1).

Immunohistochemical analysis of paraffin-embedded mammary tissues confirmed that FBLN2 protein was detected most strongly in 6-week mammary glands (Figs. 1b, 2), where it localised predominantly to the

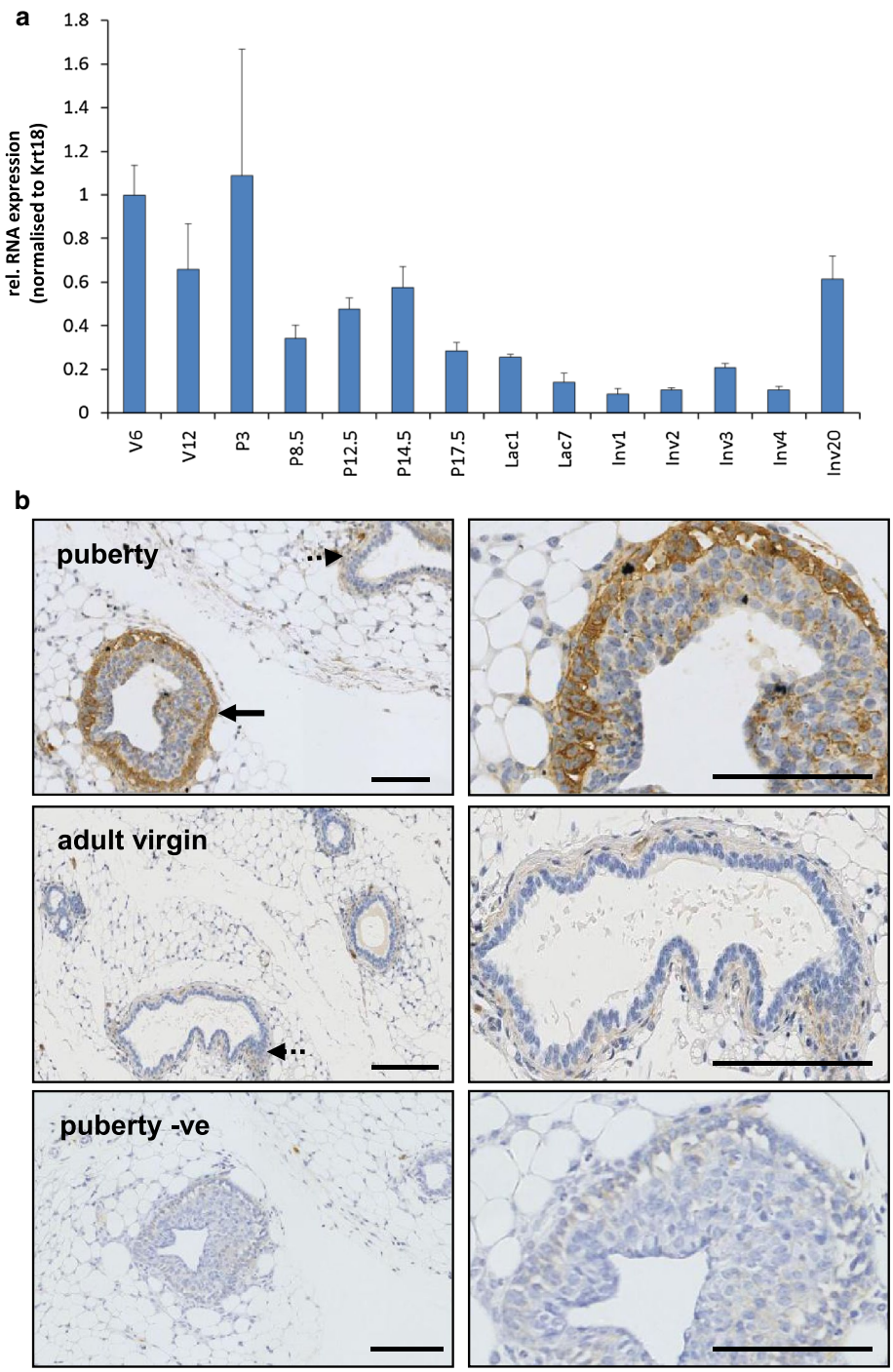

Fig. 1 Strongest FBLN2 expression is highest during puberty and early pregnancy. **a** Mean expression of *Fbln2* (relative to puberty time point) in whole glands collected at puberty 6 weeks (V6), adulthood 12 weeks (V12), pregnancy (P) days 3, 8.5, 12.5, 14.5, and 17, lactation (Lac) days 1 and 7, and involution (Inv) days 1, 2, 3, 4, and 20 measured by qRT-PCR and normalised against *Krt18*. *Error bars* represent standard deviation (SD) between three replicate PCR reactions. **b** Low and higher power images of mammary gland sections at puberty (6 weeks), adult virgin (12 weeks) and no primary antibody control (−ve) stained for FBLN2 by immunohistochemistry. FBLN2 was localised to the TEB (*solid arrows*) at six weeks and to a much lesser extent the pubertal ducts (*dotted arrow*). In the adult mammary gland weak FBLN2 expression was associated with the stroma around ducts (*dotted arrow*). *Scale bars* represent 100 μm. Mammary glands from three animals was tested for each time point

growing front of the primary epithelial network, the TEB. This strong association of FBLN2 expression with TEB epithelium was also seen when *Fbln2* RNA levels were measured by qRT-PCR in isolated TEB and ducts of a pubertal gland (Fig. 2a), and in pubertal mammary gland strips that were enriched either for TEB (Post-LN) or ducts (Pre-LN, Fig. 2b). Western blot analysis of proteins extracted from these strips showed a major ~195 kDa band that was strongest in strips enriched for TEB (Fig. 2c).

FBLN2 localises to cap cells

FBLN2 localisation was not restricted to mammary epithelium, but was also detectable in the stroma (Figs. 1b, 2d). Stromal expression was strongest in the proximal

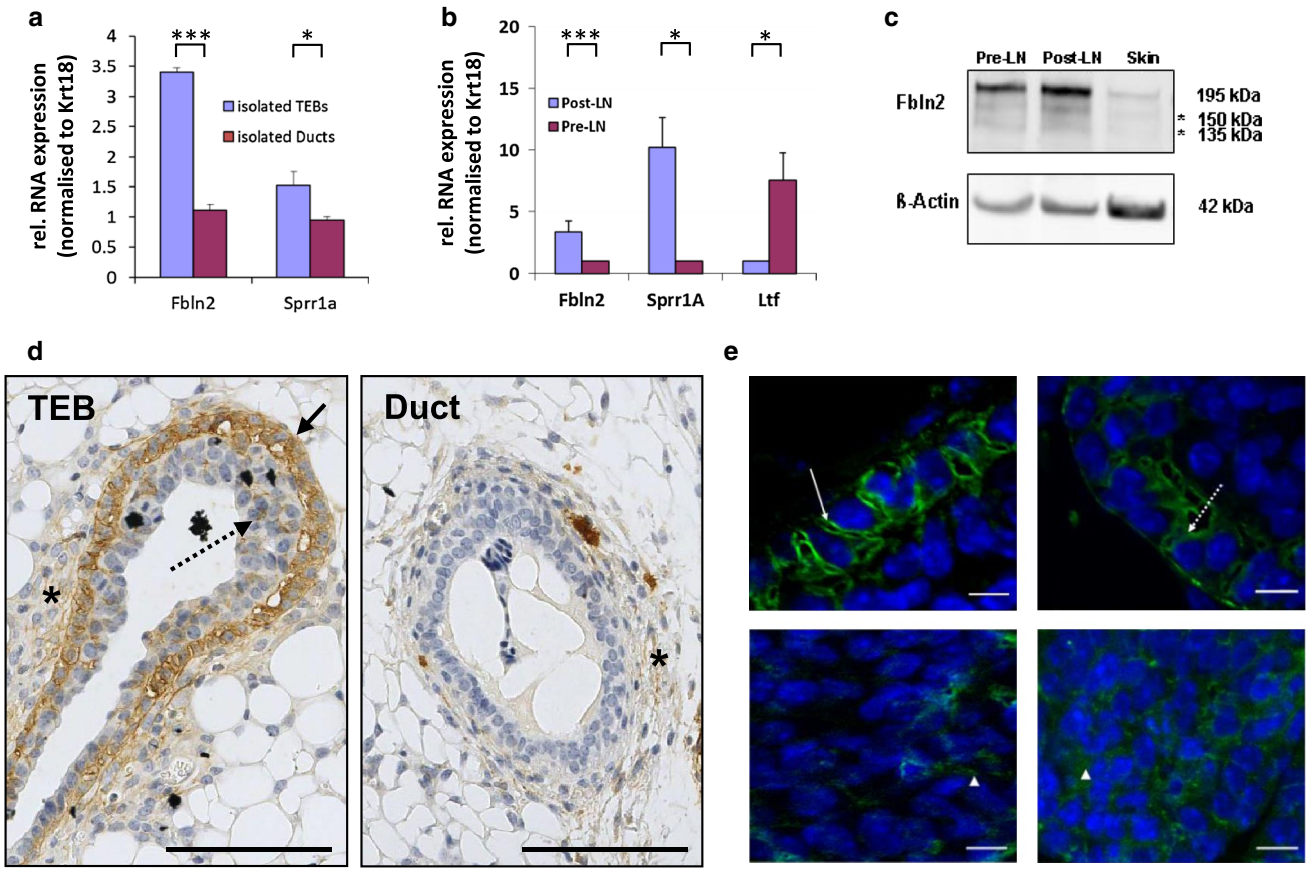

Fig. 2 FBLN2 localises to cap cells of the TEB. Relative mean expression of *Fbln2* mRNA in **a** isolated TEB and ducts and **b** in pubertal mammary tissue strips enriched for TEB (Post-LN) or ducts (Pre-LN) measured by qRT-PCR and normalised to *Krt18*. Mean expression of *Fbln2* is significantly greater in TEB than ducts. The TEB marker *Sprr1a* and ductal marker *Ltf* were used as controls for TEB or ducts as described previously [19, 51]. Samples in **a** were pooled from 300 mice (1,145 TEBS and 1,111 ducts) as described in [19] and *error bars* denote technical variability. *Error bars* in **b** indicate 95 % confidence levels for at least three qRT-PCRs using at least three independent RNA extracts from different animals. **p* value ≤0.05, ****p* value ≤0.001. **c** Western Blot for FBLN2 protein (195 kDa) using rabbit polyclonal anti-FBLN2 antibody in the Pre-LN strips, Post-LN strips and skin (positive control). The image is representative of three independent experiments. *Asterisks* denote two additional, uncharacterised bands of a lower molecular weight (150, 135 kDa), most likely proteolytic cleavage products. β-actin was used as loading control. **d** Immunohistochemical staining for FBLN2 on FFPE-tissue sections of pubertal mouse mammary glands, showing strongest FBLN2 expression in the outer cap cell layer of TEB (*black arrow*). Some protein is also detectable between body cells (*dotted arrows*) and in the stroma around TEB (*asterisk*). Expression localises to the cell membranes, cytoplasm and extracellular spaces. Very low FBLN2 levels can be detected within the stroma around ductal epithelium (*asterisk*). *Scale bars* are 100 μm. **e** FBLN2 detected by confocal immunofluorescence microscopy on FFPE-tissue sections of pubertal 6 week old mice showing detailed FBLN2 localisation to cap cell (*upper row*) membranes (*arrow*) and cytoplasm (*dashed arrow*). Body cells (*lower row*) show FBLN2 staining in the cytoplasm or extracellular spaces (*arrow heads*). *Scale bars* are 10 μm. The images are representatives of six glands examined from three animals

zone surrounding the TEB, but significant expression was also identified in the distal capsule, at the very edge of the fat pad (data not shown). Although very low amounts of FBLN2 were also present in the stroma surrounding ducts, its epithelial expression was almost exclusively associated with TEB (Table 1). Immunofluorescent staining showed that within these structures FBLN2 expression was predominantly localised to the membranes and the cytoplasm of the cap cells (Fig. 2e, supplementary Figure 2), which are the myoepithelial progenitor cells, as well as to the surrounding ECM and the newly developing myoepithelial cells. However, some non-uniform localisation was also detected in the cytoplasm or between body cells (Fig. 2e), which will later form the luminal epithelial cell layer. In comparison to the TEB (Fig. 2d), ductal epithelial expression of FBLN2 was very weak or absent, and no staining was observed in the luminal epithelium.

FBLN2 expression during early pregnancy

While RNA expression was always strongest during puberty, qRT-PCR also detected a rise in *Fbln2* epithelial

Table 1 FBLN2-staining according to the quickscore method in the pubertal mouse mammary gland

	%-Age score		Intensity score		Quickscore	
	TEB	Ducts	TEB	Ducts	TEB	Ducts
V6-1	6	5	3	1	18	5
V6-2	6	2	3	1	18	2
V6-3	6	4	3	1	18	4
V6-3	6	4	3	1	18	4

FBLN2 staining in TEB and ducts, respectively, from mammary gland sections from four 6-week old pubertal mice was semi-quantified using a combination of intensity score and percentage of structures stained according to the quickscore method [23], showing that FBLN2 expression was predominantly associated with TEB. At least 30 TEB and 75 ducts have been counted. The table shows the scores for each section

expression during early pregnancy when normalised against *Krt18*, though this increase was not found when normalised to *Krt14* (Fig. 1a, supplementary Figure 1). Immunohistochemistry confirmed increased levels of FBLN2 protein during very early pregnancy, before and as the first morphological signs of alveolar budding become visible (Fig. 3). FBLN2 protein abundance increased in the first 48 h, peaked at 72 h, but was again strongly reduced by day 4.5 (Table 2). Expression was restricted to the cell membrane and cytoplasm of the outermost, myoepithelial layer of the ductal epithelium and the surrounding stroma.

FBLN2 expression is strongly induced in the mammary gland by E2 and P priming

Since FBLN2 is induced by progesterone in the endometrial stromal cells [24], the influence of pubertal hormones on *Fbln2* mRNA expression in the mammary gland was investigated by qRT PCR. Mammary glands were collected from 4.5 week old mice primed for one week prior to collection with pellets of oestrogen (E2), oestrogen and progesterone (E2+P), or placebo. *Fbln2* mRNA was 4 fold and 3.6 fold upregulated in E2+P and E2 treated glands, respectively, compared to placebo (Fig. 4a). Immunohistochemical examination showed similar strong FBLN2 expression in the TEB and their surrounding stroma along with the ductal stroma irrespective of hormonal treatment. However, ductal epithelial expression was more prominent in E2+P treated than E2 treated mice or placebo control.

FBLN2 isoforms show differential expression in the pubertal mammary gland

Since splice variation produces two FBLN2 isoforms that differ in the presence of the third EGF-like domain (exon 9; Fig. 5a) and FBLN1 protein variants have different and sometimes opposing functions (for review see [25]), isoform expression of FBLN2 in TEB and ducts was investigated. Semi-quantitative RT-PCR confirmed that *Fbln2v1* mRNA was the most abundant isoform in TEB, while both variants were weakly present in ducts. Similar analysis of tissue strips detected slightly stronger expression of *Fbln2v1* mRNA in Post LN strips where TEB were enriched amongst their surrounding stroma, but neither of the two isoforms predominated clearly in Pre LN strips enriched for ducts and their stroma (Fig. 5b).

FBLN2 affects mammary epithelial cell–matrix interaction

Cell–matrix interactions are important for TEB outgrowth during puberty and alveolar bud formation during early pregnancy, since the extracellular matrix must be remodelled for epithelium to grow into surrounding stroma. The *Fbln2* expression profile and immunohistochemical localisation suggested that it may play a role in cellular migration and adhesion within TEB structures, as strongest expression occurs around migrating TEB and during initial bud formation during pregnancy. Over-expression of the FBLN2 V1 isoform, which was found most abundant in TEB, in FBLN2-negative HC-11 cells by transient transfection showed no difference in the speed of gap closure between FBLN2 expressing and control cells in an in vitro migration assay (scratch assay) (Fig. 6a, b). Similar results were obtained with HC-11 and EpH4 cells that had been treated with FBLN2-conditioned or control media from transfected HEK293 cells (data not shown). However, when adhesion of transfected and un-transfected HC-11 cells to different extracellular matrices was tested, presence of FBLN2 significantly increased the adhesiveness to vitronectin, tenascin, fibronectin and laminin, while adhesion to collagens I, II and IV was not significantly affected (Fig. 6c). Although Fibronectin (FN) is the best documented binding partner for FBLN2 and has the strongest binding affinity in vitro, immunofluorescence staining on serial sections of 6 week old pubertal mammary glands (Fig. 6d) showed no co-localisation of these two proteins, as FBLN2 was mostly detected in TEB and their surrounding stroma, whereas FN was most detected around ducts.

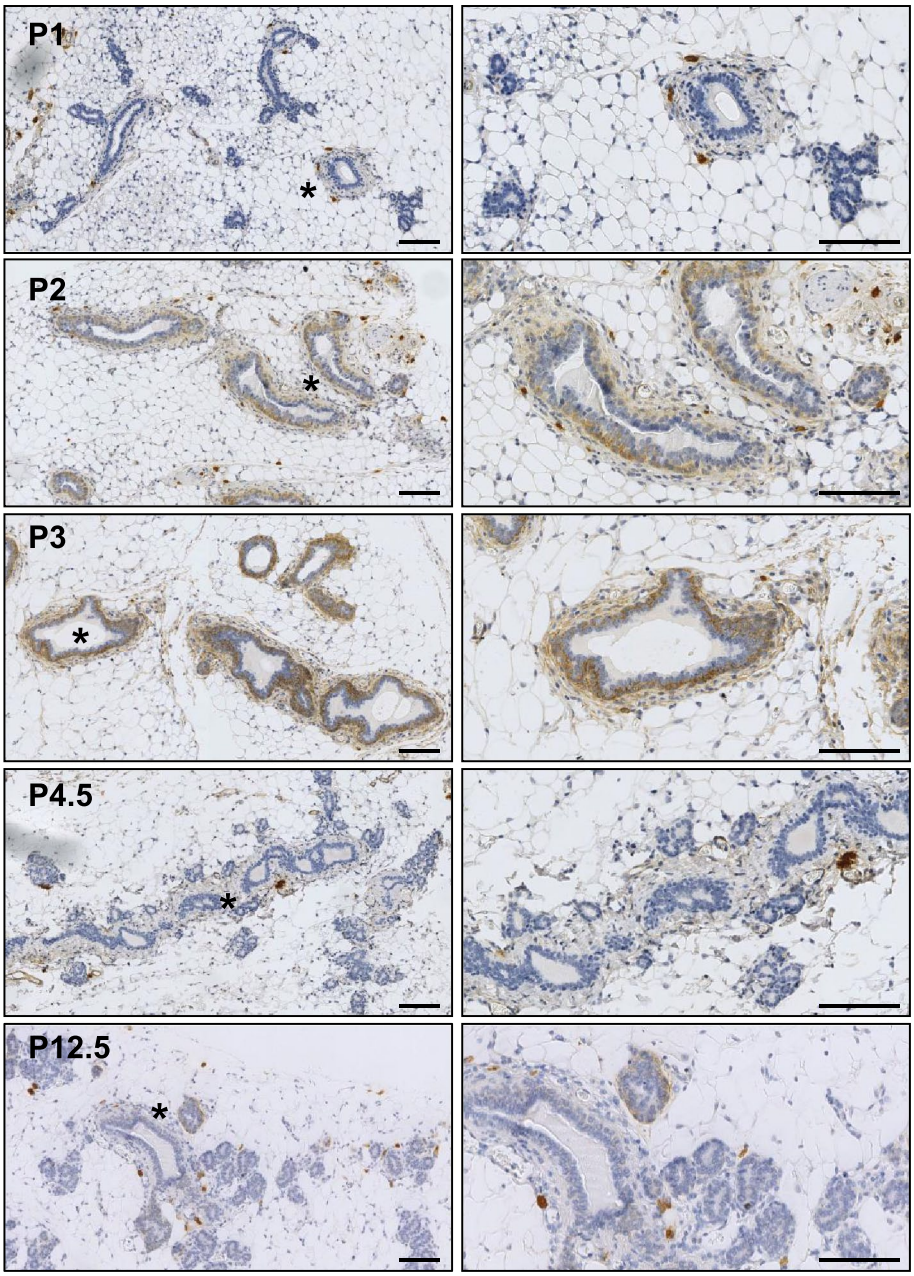

Fig. 3 FBLN2 is expressed during early pregnancy. FBLN2 localisation by immunohistochemistry of tissue sections of mouse mammary glands obtained from pregnant mice at 24 h (*P1*), 48 h (*P2*), 72 h (*P3*), 4.5 days (*P4.5*) and 12.5 days (*P12.5*). *Right hand* images show higher magnification of areas marked by *asterisk* in *left hand* images. FBLN2 expression starts to increase 48 h after conception, peaks at 72 h and is mostly absent by pregnancy day 4.5 although some residual staining is noted at 12.5 days. *Scale bars* are 100 μm. Glands from three animals were examined per developmental stage

FBLN2 co-localises with versican in cap cells and during early pregnancy

FBLN2 is highly expressed in the developing embryonic heart where it is colocalises with the proteoglycan versican (VCAN) and hyaluronan in the endocardial cushion tissue [26], which expresses smooth-muscle actin. Furthermore, FBLN2 can bind and crosslink VCAN/hyaluronan complexes and FBLN2/VCAN interactions are required for smooth muscle cell migration [16]. Since the ECM around TEB cap cells consists largely of hyaluronan, and analysis of our previous expression data of mammary gland development [20] showed preferential expression of VCAN during puberty and early pregnancy (Fig. 7a), we tested whether VCAN colocalised with FBLN2 around TEB. Using RNA from post-lymph and pre-lymph node strips from pubertal mammary glands *Vcan* RNA showed variable but consistent up-regulation in the TEB-enriched tissue strips in three independent experiments (Fig. 7b). Immunohistochemical analysis of pubertal and early pregnant mouse glands revealed that FBLN2 and VCAN showed identical staining patterns in consecutive sections (Fig. 7b; Supplementary Figure 3), including preferential staining of what morphologically appears to be a mammary ductal side bud (Supplementary Figure 4), indicating co-localisation of the two proteins. The major component of the basal lamina,

Table 2 FBLN2-staining according to the quickscore method in the adult virgin and pregnant mouse mammary gland

	%-Age score	Intensity score	Quickscore
V10-1	1	0	0
V10-2	1	1	1
V10-3	2	1	2
V12-1	1	2	2
V12-2	1	0	0
V12-3	1	3	
P1-1	1	0	0
P1-2	1	3	3
P1-3	1	0	0
P2-1	6	2	12
P2-2	1	3	3
P2-3	5	2	10
P3-1	4	2	8
P3-2	6	3	18
P3-3	6	3	18
P4.5-1	1	0	0
P4.5-2	1	0	0
P4.5-3	2	3	6
P8.5-1	1	0	0
P8.5-2	1	0	0
P8.5-3	1	2	2
P12.5-1	1	0	0
P12.5-2	1	0	0
P12.5-3	1	0	0
P14.5-1	2	1	2
P14.5-2	1	0	0
P17.5-1	1	0	0
P17.5-2	1	0	0
P17.5-3	1	0	0

FBLN2 staining was semi-quantified in mammary gland sections from adult virgin (10 week and 12 week) mice and from days 1, 2, 3, 4.5, 8.5, 12.5, 14.5 and 17.5 of pregnancy. The table shows the quickscores for each section. Each section contained at least 20 ducts

laminin-111 (LN111) also showed a similar if weaker staining pattern (Supplementary Figure 3).

Loss of FBLN2 is compensated by increased protein levels of FBLN1 around the TEB

To establish whether FBLN2 is essential for mammary gland development, we compared ductal morphologies of wild type and *Fbln2* KO mice [18]. Immunohistochemical evaluation confirmed that pubertal KO mice did not express FBLN2, while controls showed the typical staining pattern in TEB cap and body cells (Fig. 8a). However, morphological assessment of the glands at three weeks (pre-puberty) and six weeks (puberty) both as wholemounts (Fig. 8b) and H&E sections (data not shown) failed to detect any obvious differences between *Fbln2* KO and control mice. The length and degree of branching of the ductal tree appeared similar and although the TEB appeared slightly smaller in wholemounts of *Fbln2* KO mice, this was not supported on examination of tissue sections (data not shown).

Since compensatory local up-regulation through re-localisation of FBLN1 protein has previously been reported in the inner elastic lamina of the aorta of *Fbln2* KO mice, we examined the expression of FBLN1 in pubertal transgenic and control mammary glands (Fig. 8c). While expression of FBLN1 in the control mice was only weak and diffuse throughout epithelium and stroma, FBLN1 staining was distinctly increased in the *Fbln2* KO mice, with FBLN1 staining clearly visible within and around the TEB (cytoplasm and extracellular spaces of body cells and cell membranes and cytoplasm of cap cells), their basement membrane and surrounding stroma, where FBLN2 is normally found. These data indicate that, as in the aorta, a possible compensatory up-regulation of *Fbln1* around and within the TEB takes place.

Discussion

Cell–matrix interactions are crucial for controlling mammary epithelial outgrowth and branching morphogenesis during puberty, and budding/tertiary branching during pregnancy [1]. Here, we have described the glycoprotein FBLN2 as a novel component of the TEB-associated cap cell epithelium and of the myoepithelium during very early pregnancy when the first morphological changes become microscopically visible. Our results on tissue distribution, hormonal regulation and timing of FBLN2 expression in the mammary gland suggest that FBLN2 may be involved in the ECM remodeling process that allows epithelial growth into the surrounding stroma. The mechanism(s) by which FBLN2 might function in the mammary gland is as yet unknown. However, the possible in vivo compensatory up-regulation/re-localisation of FBLN1 indicates that this mechanistic function may be conserved between fibulin family members.

Although its function in the mammary gland is not yet understood, our findings that FBLN2 and VCAN were both preferentially expressed in the mammary gland during times of epithelial expansion in TEB-enriched tissue and co-localised specifically in cap cells, which have recently been confirmed by lineage-tracing to represent the myoepithelial progenitor cells [27], and in the myoepithelium just before pregnancy-associated budding occurs (days 2–3) appear highly significant. Concordingly, microarray data for *Vcan* RNA also showed a similar up-regulation during puberty and early pregnancy (Fig. 7a), indicating that FBLN2 and VCAN may act together to prepare the ECM

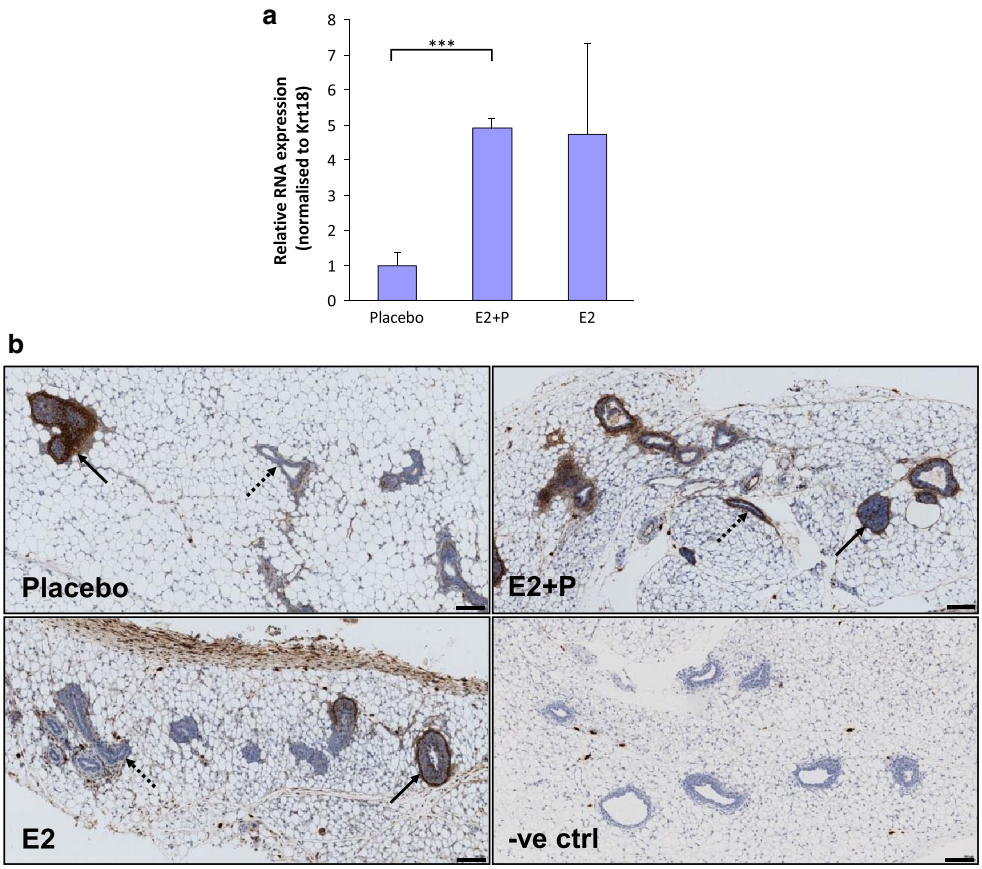

Fig. 4 FBLN2 expression can be hormonally induced in mouse mammary gland. **a** *Fbln2* mRNA levels relative to *Krt18* in mammary glands of 4.5 weeks old mice that were hormone primed with either placebo, oestrogen-progesterone (E2 + P) or oestrogen (E2) pellets. *Error bars* show 95 % confidence levels. ***p value ≤ 0.001. $n = 3$ (placebo and E2 + P), $n = 4$ (E2). **b** Sections of mammary gland from 4.5 week old mice primed with placebo, E2+P and E2 hormone pellets for 1 week prior to tissue collection and stained with anti-FBLN2 antibody. No primary antibody control (*−ve ctrl*) shows no staining in the epithelium of E2 + P treated mice. *Solid arrows* denote TEB and *dotted arrows* indicate ducts. At least three mice were studied for each treatment. *Scale bars* are 100 μm

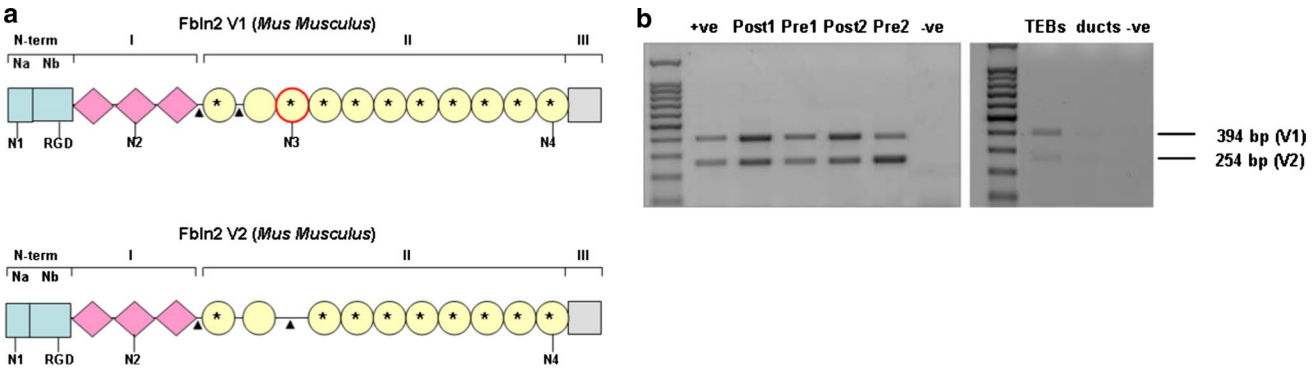

Fig. 5 Both FBLN2 variants are expressed in the mammary gland. **a** Murine FBLN2 consists of N-terminus domain (N-term), anaphylatoxin motifs in domain I, EGF-like repeats in domain II and C-terminal domain (III). FBLN2 V1 and FBLN2 V2 differ only by the absence in FBLN2 V2 of the EGF-like domain 3, which is encoded by exon 9 (*circle* with a *red outline*) and a potential glycosylation site (N3). *Circles* with an *asterisk* possess a Ca^{2+} binding consensus sequence. Amino acid linkers (*arrow heads*) join the first EGF-like repeat to domain I and other EGF-like repeat domains. Positions of potential N-glycosylation sites (N1, N2, N3 and N4) and the RGD consensus (RGD) are indicated. **b** PCR illustrating expression of both splice variants *Fbln2* V1 (394 bp) and V2 (254 bp) in Post-LN and Pre-LN strips and isolated TEB (RNA was pooled from 1145 TEB before cDNA synthesis) with weak product from ducts. Positive control is cDNA from mouse kidney and negative is no RT PCR quality control. Tissue strips were collected from individual mice for each RNA isolate. The figure shows two results representative of four independent RNA isolates

for the new epithelial outgrowth. In the mammary gland VCAN and FBLN2 were both down-regulated after early pregnancy (Fig. 7c), indicating that they may only be involved in growth initiation and pubertal ductal expansion. VCAN can bind hyaluronan, which is highly abundant around cap cells [28], and its receptor CD44 [29, 30]. A hyaluronan/VCAN-rich pericellular matrix is required for vascular smooth muscle cell proliferation and migration

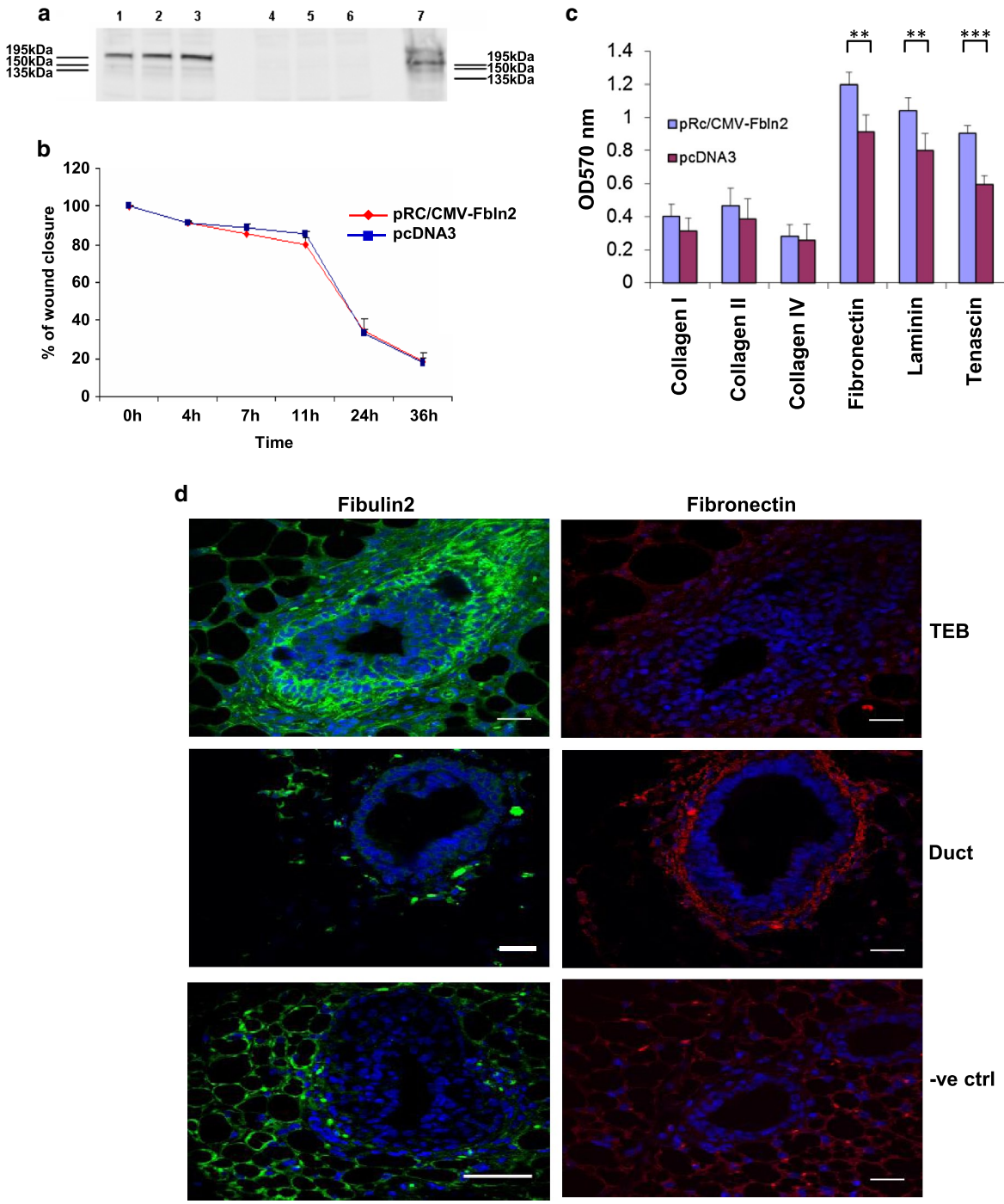

Fig. 6 FBLN2 over-expression enhances adhesion to ECM but does not colocalise with fibronectin. **a** Western blot showing FBLN2 over-expression in HC-11 cells transfected with pRc/CMV-*Fbln2* (*lanes* 1–3; three independent transfections) compared to pcDNA3 transfected cells (*lanes* 4–6; three independent transfections). Proteins were isolated from the cells at the end of the migration assay shown in **b**. NIH3T3 cells were used as positive control (*lane* 7). **b** Graph illustrating the percent of gap closure in HC-11 cells transfected with pRc/CMV-*Fbln2* or pcDNA3. Assay performed on confluent cells (48 h after transfections). No difference in the speed of cell migration was noted in FBLN2 expressing HC-11 cells in comparison to empty vector transfected HC-11 cells. Results from triplicate experiments are shown, with *error bars* showing 95 % confidence intervals. **c** Cell adhesion assay to ECM proteins for HC-11 cells either transfected with pRc/CMV-*Fbln2* or pcDNA3 vectors for 24 h. Blank wells were coated with BSA. ***p* value ≤0.01, ****p* value ≤0.001. Cells seeded in triplicate for each experimental condition. *Error bars* represent SD. **d** Confocal images of immunofluorescence staining for FBLN2 and FN in consecutive sections of pubertal mouse mammary gland epithelium and stroma. Transverse sections through a 6 week mouse mammary gland showing TEB (*top row*) and duct (*middle row*) stained with anti-FBLN2 (*green*) or anti-FN (*red*) antibodies and nuclear DAPI (*blue*). No primary antibody control shown in *bottom row*. *Scale bars* are 50 μm. Mammary glands from at least three mice were used

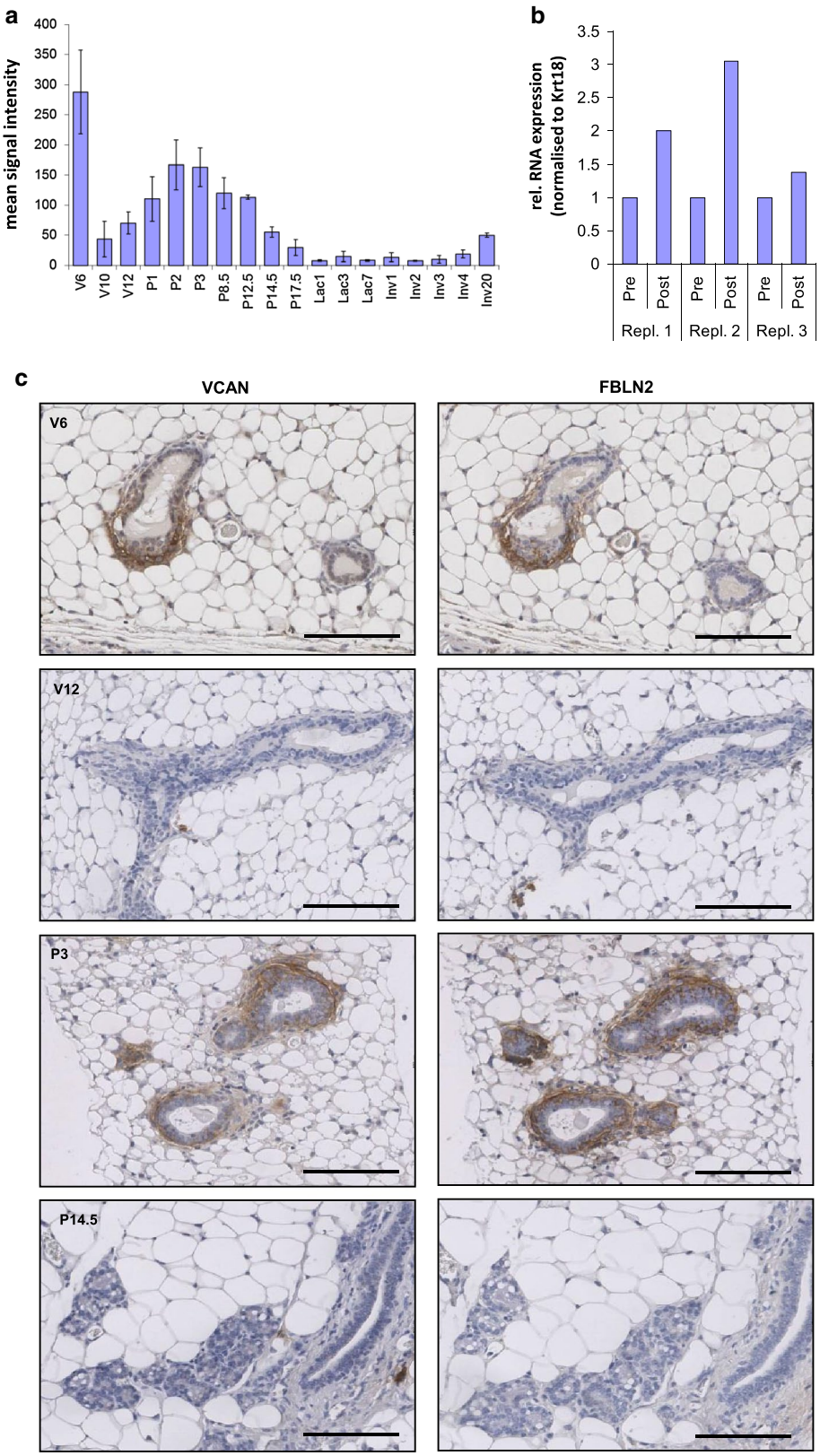

Fig. 7 Versican RNA and protein abundance in the mammary gland. **a** Versican (*Vcan*) RNA expression measured by microarray analysis [20] showing highest abundance during puberty and early pregnancy. Values represent the mean signal intensities normalised to the overall chip intensities *Error bars* show SD of independent triplicates. **b** Three independent extracts of post-LN and Pre-LN strips were assessed for *Vcan* RNA abundance by qRT-PCR and normalised to *Krt18*. *Vcan* showed variable but consistent increased expression in the Post-LN strips. **c** Immunohistochemical analysis of FBLN2 and VCAN localisation in consecutive FFPE-sections pubertal, adult virgin, early pregnancy, and mid pregnancy mammary glands. FBLN2 and VCAN showed nearly identical staining patterns, with preferential expression in and around cap cells and in myoepithelial cells during early pregnancy, but very low expression in subtending pubertal ducts, or in glands from adult virgin or mid-pregnant glands. Images are representative of results from three independent glands. *Scale bars* are 100 μm

in vitro [31]. FBLN2 can bind and crosslink VCAN/hyaluronan complexes [32], and these FBLN2/VCAN interactions are required for smooth muscle cell migration and proliferation during development and in response to injury [16]. In the developing heart, FBLN2 is highly expressed and colocalises with VCAN and hyaluronan in endocardial

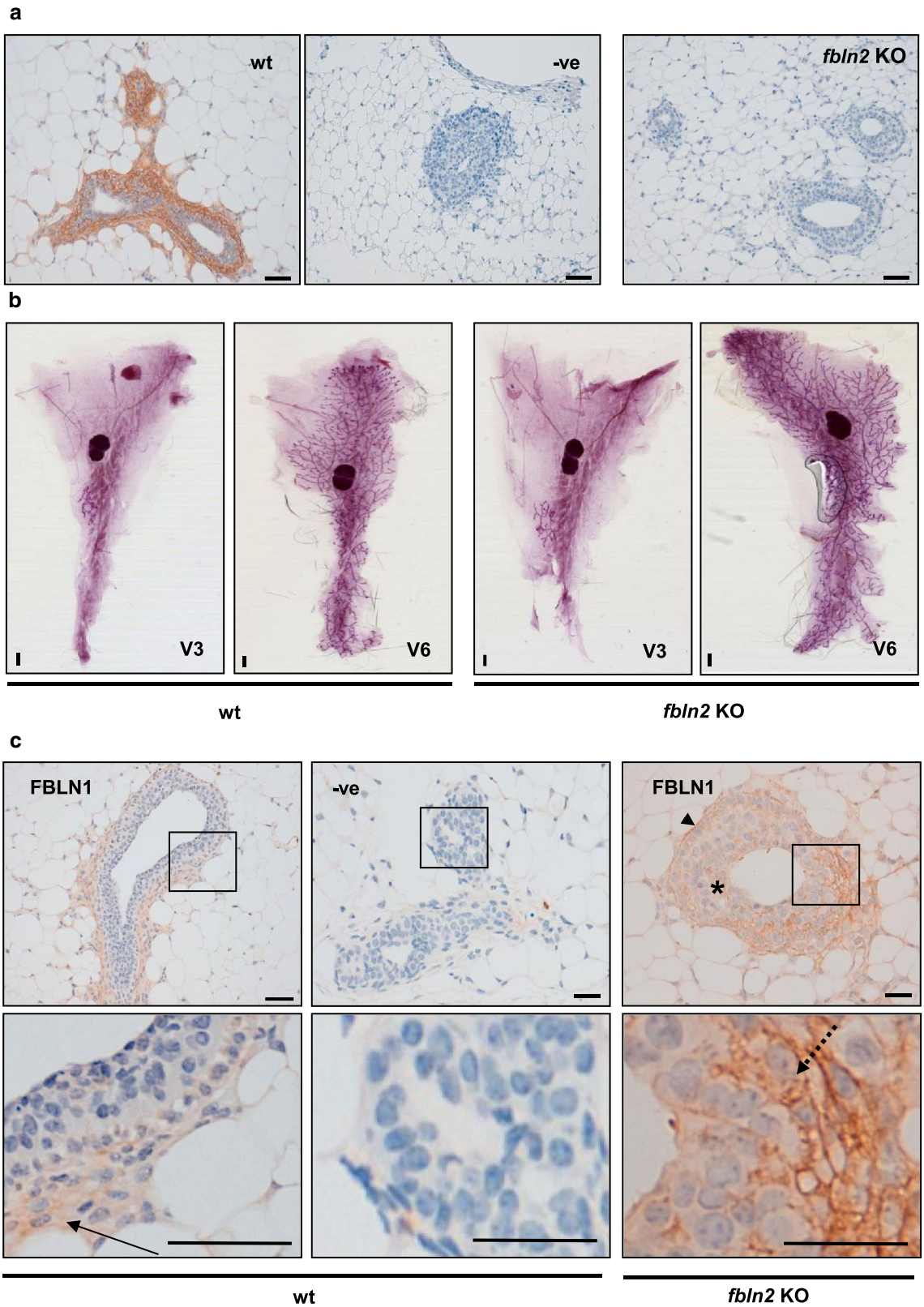

cushion tissue [26, 33], and *Vcan* KO mice [heart defect (*hdf*) mice] lack normal cardiac development and die at around embryonic day 10.5 [34]. It will be interesting to establish whether a conditional *Vcan* KO mouse using, e.g., a *CK14-Cre* model shows the predicted mammary developmental phenotype. Interestingly, similarities between events

◂**Fig. 8** *Fbln2* KO mice have no obvious mammary phenotype but express higher levels of FBLN1. **a** FBLN2 stained sections from six week mammary glands collected from wild type (*wt*) and *Fbln2* KO mice (*Fbln2 KO*). No FBLN2 staining was detected in the no-primary antibody control (−ve) or in *Fbln2* KO mouse mammary glands whereas prominent FBLN2 expression was seen in wt epithelium. *Scale bars* are 50 μm. 3 *Fbln2* KO and 3 wt mice were examined. **b** Representative carmine alum stained wholemounts from 3 week and 6 week wt (*left panel*) and *Fbln2* KO (*right panel*) mice. *Scale bars* are 1 mm. **c** Up-regulation of FBLN1 in the epithelium of *Fbln2* KO pubertal mouse mammary glands. Mammary glands of pubertal 6 week wt (*wt*) and *Fbln2* KO (*Fbln2 KO*) mice showing TEB epithelium stained with anti-FBLN1 (*Fbln1*) or no primary FBLN1 antibody (−*ve*). The *lower row* shows the corresponding magnified areas of each image. Weak FBLN1 staining in wt glands was contained in the stroma around TEB (*arrow*). In *Fbln2* KO glands, however, FBLN1 was strongly detectable, localising to the basement membrane (*arrow head*), cap cells (*dotted arrow*) and cytoplasm and extracellular spaces between body cells (*asterisk*), in similar locations to those seen for FBLN2 in wt pubertal mouse mammary glands. *Scale bars* are 50 μm (wt) and 25 μm (KO). $n = 3$ animals

of endocardial cushion tissue formation and mammary epithelial branching have recently been described with regard to matrix metalloprotease activity and EMT [35]. Previous speculation has suggested FBLN2 links VCAN to microfibrils; however, recent evidence shows that VCAN directly interacts with microfibrils [11, 36, 37].

The cap cells, which are the myoepithelial progenitor cells, form a continuous layer of epithelial cells while proliferating and forming the new myoepithelium, thereby allowing the ductal epithelium to move forward and invade the surrounding fat pad [38]. Increased FBLN2 levels are similarly found within the ECM surrounding embryonic smooth muscle precursor cells of developing aortic arch vessels, which proliferate to form a multilayered structure [39]. FBLN2 acts as a marker of smooth muscle precursor cells and is closely linked to proliferation and differentiation. It has been speculated that these cells may form an ECM and protein scaffold in which they can proliferate and differentiate into smooth muscle cells under optimal conditions [39]. Parallels could be made for the ECM around cap cells, which need to proliferate and differentiate into smooth muscle actin-positive myoepithelial cells. In the vascular system, *Fbln2* transcription is down regulated once a basic framework of alternating ECM layers is formed [39], and this mimicks the expression of FBLN2 in mammary gland during puberty and early pregnancy and its down-regulation thereafter. One could speculate that the myoepithelial cells of pregnancy-associated budding may resemble cap cells of the TEB during this growth initiation phase. Interestingly, *Vcan* RNA was recently found to be expressed in FACS-sorted mammary basal epithelial stem/progenitor cells and was down-regulated in these cells as part of a parity-induced gene signature [40]. FBLN2 was similarly significantly down-regulated ($p < 0.001$) in the basal stem/progenitor cell population from mice which had gone through a full term pregnancy compared to age-matched virgin control mice (Meier-Abt, personal communication), further strengthening our hypothesis that FBLN2 and VCAN both may play important roles in epithelial outgrowth. Although these data strongly support expression of *Fbln2* mRNA within the mammary (myo-)epithelium, expression within the stroma, particularly endothelial cells and fibroblasts is highly likely, as FBLN2 protein was found within the stromal capsule surrounding the mammary fat pad, and we cannot rule out that at least part of the FBLN2 seen around the mammary epithelium is of fibroblastic origin.

Despite its specific localisation within the developing mammary gland and association with basal stem/progenitor cells, loss of FBLN2 in KO mice did not result in a mammary phenotype. Comparable ductal tree development, TEB number and morphology were noted in WT and FBLN2 deficient mice. A similar observation was noted previously for general mouse development in which FBLN2 was found to be dispensable [18]. *Fbln2* KO mice showed normal elastogenesis, development and fertility with no dysfunction in elastic fibre assembly [18]. The lack of a developmental phenotype most likely resulted from compensatory up regulation of FBLN1 which was present in locations where FBLN2 ought to have been detected, but not in WT controls. FBLN1 binds to the same ECM proteins as FBLN2 such as VCAN, laminin, nidogen, and fibronectin [8, 9], and we have shown increased FBLN1 protein levels around the TEB in *Fbln2* KO mice where FBLN2 was found in WT animals (Fig. 8) indicating that compensatory expression of *Fbln1* may rescue a possible *Fbln2* KO phenotype, as shown previously [18]. Other fibulins may also compensate since double knockout mice for *Fbln2* and *Fbln5* genes have a more severe phenotype (disorganisation of elastic lamina of blood vessels) not seen in either of the single knockouts [41]. Since *Fbln1* KO mice are lethal due to haemorrhage from small blood vessels with defective BM [42], a conditional knockout for *Fbln1* on the *Fbln2* KO background would be required to test its effect in the mammary gland. Nevertheless, the fact that a compensatory mechanism exists for lack of FBLN2 leads us to speculate that fibulins may be critical for mammary morphogenesis.

In our migration assay, over expressed FBLN2 did not alter migration of HC-11 cells, though different results might be obtained with myoepithelial cells, as FBLN2 increases migration of smooth muscle cells in response to injury in vitro [16] and is upregulated in migrating mesenchymal cells of cardiac valves and aortic arch vessels during EMT [39]. Within TEB, FBLN2 could influence the migration of the multicellular structure, not by affecting single cell migration, but by maintaining adhesion between

cap cells and the ECM and/or strengthening the BM by binding and cross-linking with other ECM proteins, including VCAN, which would be consistent with its RGD site and its ability to promote adhesiveness of mammary cell lines to ECM coated surfaces [43].

FBLN2 has at least 14 known binding partners, 12 of which are located in the ECM with the remaining two, integrin β3 (ITGB3) and integrin α5 (ITGA5) acting as membrane receptors for FBLN2 (Supplementary Figure 4). The diverse molecular interactions of FBLN2 suggest that it is involved in stabilising the organisation of ECM structures such as BM, elastic fibres and the FN matrix [8–10, 41]. FBLN2 localised to the BM of TEB where LN111 forms one of the main constituents [44]. FBLN2 interacts with LN111 and LN332 in vitro [9, 45] and FBLN2 increased the adhesiveness of HC-11 cells to laminin in our study. LN111 is essential for normal TEB development in puberty, with fewer TEB and consequently reduced ductal outgrowth in mouse mammary glands implanted with pellets containing LN111 or integrin β1 function perturbing antibodies [46]. Hence, as a binding partner of LN111, FBLN2 may contribute to the stabilisation of the BM network and contribute to the maintenance of TEB structure during morphogenesis. A similar role for FBLN2 in basement membrane integrity has recently been described in the mouse skin as *Fbln2* KO mice phenocopied a perinatal skin blistering phenotype of epidermal integrin α3β1-deficient mice [47]. Despite increasing the adhesiveness of HC-11 to FN in our study, FBLN2 did not appear to colocalise with FN in mammary stroma, suggesting they are not binding partners during TEB outgrowth.

In addition to the proposed structural role for FBLN2 within the developing ECM/cap cells, fibulins, including FBLN2, also compete for fibrillin-1 binding sites with latent transforming growth factor-binding protein latent TGFβ binding protein 1 (LTBP1) [48]. Since the latter is necessary for TGFβ signalling and regulation [49], and since FBLN2 has previously been shown to affect TGFβ-signalling in angiotensin II-induced cardiac hypertrophy [50], it is conceivable that FBLN2 may also affect TGFβ activity around the outgrowing mammary epithelium. Given the potential importance of such a regulatory system, further studies appear justified to test this hypothesis.

Conclusion

Our results suggest that, similar to the vascular remodelling during embryonic development, FBLN2 is involved in the very early development and/or remodelling of the ECM around myoepithelial cells of the mouse mammary gland. These results shed new light on the early morphological changes that occur during epithelial budding at early pregnancy and propose for the first time a role for fibulins in mammary gland morphogenesis.

Acknowledgments The authors would like to thank Drs. Meier-Abt and Momo Bentires-Alj for sharing unpublished data, Dr JM Iglesias for sharing his technical expertise, and Jennifer Joyce for her technical assistance and providing the whole-mounts of the *Fbln2* KO mice. All animal work was carried out under personal licence PIL 60/11179 and project licence PPL 60/3712 and was approved by the University of Glasgow ethics committee. The work was funded by a Breakthrough Breast Cancer project grant to BAG, who designed the initial study, and by the Egyptian Ministry for Higher Education to AMI and TS.

Conflict of interest The authors declare that they have no conflict of interest.

References

1. Muschler J, Streuli CH (2010) Cell-matrix interactions in mammary gland development and breast cancer. Cold Spring Harb Perspect Biol 2:a003202
2. Daniel CW, Silberstein GB, Strickland P (1987) Direct action of 17 beta-estradiol on mouse mammary ducts analyzed by sustained release implants and steroid autoradiography. Cancer Res 47:6052–6057
3. Green KA, Lund LR (2005) ECM degrading proteases and tissue remodelling in the mammary gland. BioEssays 27:894–903
4. Argraves WS, Dickerson K, Burgess WH, Ruoslahti E (1989) Fibulin, a novel protein that interacts with the fibronectin receptor beta subunit cytoplasmic domain. Cell 58:623–629
5. Roark EF, Keene DR, Haudenschild CC, Godyna S, Little CD et al (1995) The association of human fibulin-1 with elastic fibers: an immunohistological, ultrastructural, and RNA study. J Histochem Cytochem 43:401–411
6. Miosge N, Gotz W, Sasaki T, Chu ML, Timpl R et al (1996) The extracellular matrix proteins fibulin-1 and fibulin-2 in the early human embryo. Histochem J 28:109–116
7. de Vega S, Iwamoto T, Yamada Y (2009) Fibulins: multiple roles in matrix structures and tissue functions. Cell Mol Life Sci 66:1890–1902
8. Kobayashi N, Kostka G, Garbe JH, Keene DR, Bachinger HP et al (2007) A comparative analysis of the fibulin protein family. Biochemical characterization, binding interactions, and tissue localization. J Biol Chem 282:11805–11816
9. Sasaki T, Gohring W, Pan TC, Chu ML, Timpl R (1995) Binding of mouse and human fibulin-2 to extracellular matrix ligands. J Mol Biol 254:892–899
10. Sasaki T, Wiedemann H, Matzner M, Chu ML, Timpl R (1996) Expression of fibulin-2 by fibroblasts and deposition with fibronectin into a fibrillar matrix. J Cell Sci 109(Pt 12):2895–2904
11. Reinhardt DP, Sasaki T, Dzamba BJ, Keene DR, Chu ML et al (1996) Fibrillin-1 and fibulin-2 interact and are colocalized in some tissues. J Biol Chem 271:19489–19496
12. Loveland K, Schlatt S, Sasaki T, Chu ML, Timpl R et al (1998) Developmental changes in the basement membrane of the normal and hypothyroid postnatal rat testis: segmental localization of fibulin-2 and fibronectin. Biol Reprod 58:1123–1130
13. Zhang RZ, Pan TC, Zhang ZY, Mattei MG, Timpl R et al (1994) Fibulin-2 (FBLN2): human cDNA sequence, mRNA expression, and mapping of the gene on human and mouse chromosomes. Genomics 22:425–430

14. Ng KM, Catalano MG, Pinos T, Selva DM, Avvakumov GV et al (2006) Evidence that fibulin family members contribute to the steroid-dependent extravascular sequestration of sex hormone-binding globulin. J Biol Chem 281:15853–15861
15. Fassler R, Sasaki T, Timpl R, Chu ML, Werner S (1996) Differential regulation of fibulin, tenascin-C, and nidogen expression during wound healing of normal and glucocorticoid-treated mice. Exp Cell Res 222:111–116
16. Ström A, Olin AI, Aspberg A, Hultgardh-Nilsson A (2006) Fibulin-2 is present in murine vascular lesions and is important for smooth muscle cell migration. Cardiovasc Res 69:755–763
17. Okabe M, Ikawa M, Kominami K, Nakanishi T, Nishimune Y (1997) 'Green mice' as a source of ubiquitous green cells. FEBS Lett 407:313–319
18. Sicot FX, Tsuda T, Markova D, Klement JF, Arita M et al (2008) Fibulin-2 is dispensable for mouse development and elastic fiber formation. Mol Cell Biol 28:1061–1067
19. Morris JS, Stein T, Pringle MA, Davies CR, Weber-Hall S et al (2006) Involvement of axonal guidance proteins and their signaling partners in the developing mouse mammary gland. J Cell Physiol 206:16–24
20. Stein T, Morris JS, Davies CR, Weber-Hall SJ, Duffy M-A et al (2004) Involution of the mouse mammary gland is associated with an immune cascade and an acute-phase response, involving LBP, CD14 and STAT3. Breast Cancer Res 6:R75–R91
21. Pan TC, Sasaki T, Zhang RZ, Fassler R, Timpl R et al (1993) Structure and expression of fibulin-2, a novel extracellular matrix protein with multiple EGF-like repeats and consensus motifs for calcium binding. J Cell Biol 123:1269–1277
22. Sasaki T, Kostka G, Gohring W, Wiedemann H, Mann K et al (1995) Structural characterization of two variants of fibulin-1 that differ in nidogen affinity. J Mol Biol 245:241–250
23. Detre S, Saclani Jotti G, Dowsett M (1995) A "quickscore" method for immunohistochemical semiquantitation: validation for oestrogen receptor in breast carcinomas. J Clin Pathol 48:876–878
24. Okada H, Nakajima T, Yoshimura T, Yasuda K, Kanzaki H (2003) Microarray analysis of genes controlled by progesterone in human endometrial stromal cells in vitro. Gynecol Endocrinol 17:271–280
25. Gallagher WM, Currid CA, Whelan LC (2005) Fibulins and cancer: friend or foe? Trends Mol Med 11:336–340
26. Miosge N, Sasaki T, Chu ML, Herken R, Timpl R (1998) Ultrastructural localization of microfibrillar fibulin-1 and fibulin-2 during heart development indicates a switch in molecular associations. Cell Mol Life Sci 54:606–613
27. Van Keymeulen A, Rocha AS, Ousset M, Beck B, Bouvencourt G et al (2011) Distinct stem cells contribute to mammary gland development and maintenance. Nature 479:189–193
28. Silberstein GB, Daniel CW (1982) Glycosaminoglycans in the basal lamina and extracellular matrix of the developing mouse mammary duct. Dev Biol 90:215–222
29. Kawashima H, Hirose M, Hirose J, Nagakubo D, Plaas AH et al (2000) Binding of a large chondroitin sulfate/dermatan sulfate proteoglycan, versican, to L-selectin, P-selectin, and CD44. J Biol Chem 275:35448–35456
30. Bajorath J, Greenfield B, Munro SB, Day AJ, Aruffo A (1998) Identification of CD44 residues important for hyaluronan binding and delineation of the binding site. J Biol Chem 273:338–343
31. Evanko SP, Angello JC, Wight TN (1999) Formation of hyaluronan- and versican-rich pericellular matrix is required for proliferation and migration of vascular smooth muscle cells. Arterioscler Thromb Vasc Biol 19:1004–1013
32. Olin AI, Morgelin M, Sasaki T, Timpl R, Heinegard D et al (2001) The proteoglycans aggrecan and Versican form networks with fibulin-2 through their lectin domain binding. J Biol Chem 276:1253–1261
33. Zhang HY, Chu ML, Pan TC, Sasaki T, Timpl R et al (1995) Extracellular matrix protein fibulin-2 is expressed in the embryonic endocardial cushion tissue and is a prominent component of valves in adult heart. Dev Biol 167:18–26
34. Mjaatvedt CH, Yamamura H, Capehart AA, Turner D, Markwald RR (1998) The Cspg2 gene, disrupted in the hdf mutant, is required for right cardiac chamber and endocardial cushion formation. Dev Biol 202:56–66
35. Radisky ES, Radisky DC (2010) Matrix metalloproteinase-induced epithelial-mesenchymal transition in breast cancer. J Mammary Gland Biol Neoplasia 15:201–212
36. Isogai Z, Aspberg A, Keene DR, Ono RN, Reinhardt DP et al (2002) Versican interacts with fibrillin-1 and links extracellular microfibrils to other connective tissue networks. J Biol Chem 277:4565–4572
37. Ohno-Jinno A, Isogai Z, Yoneda M, Kasai K, Miyaishi O et al (2008) Versican and fibrillin-1 form a major hyaluronan-binding complex in the ciliary body. Invest Ophthalmol Vis Sci 49:2870–2877
38. Williams JM, Daniel CW (1983) Mammary ductal elongation: differentiation of myoepithelium and basal lamina during branching morphogenesis. Dev Biol 97:274–290
39. Tsuda T, Wang H, Timpl R, Chu ML (2001) Fibulin-2 expression marks transformed mesenchymal cells in developing cardiac valves, aortic arch vessels, and coronary vessels. Dev Dyn 222:89–100
40. Meier-Abt F, Milani E, Roloff T, Brinkhaus H, Duss S et al (2013) Parity induces differentiation and reduces Wnt/Notch signaling ratio and proliferation potential of basal stem/progenitor cells isolated from mouse mammary epithelium. Breast Cancer Res 15:R36
41. Chapman SL, Sicot FX, Davis EC, Huang J, Sasaki T et al (2010) Fibulin-2 and fibulin-5 cooperatively function to form the internal elastic lamina and protect from vascular injury. Arterioscler Thromb Vasc Biol 30:68–74
42. Kostka G, Giltay R, Bloch W, Addicks K, Timpl R et al (2001) Perinatal lethality and endothelial cell abnormalities in several vessel compartments of fibulin-1-deficient mice. Mol Cell Biol 21:7025–7034
43. Pfaff M, Sasaki T, Tangemann K, Chu ML, Timpl R (1995) Integrin-binding and cell-adhesion studies of fibulins reveal a particular affinity for alpha IIb beta 3. Exp Cell Res 219:87–92
44. Maller O, Martinson H, Schedin P (2010) Extracellular matrix composition reveals complex and dynamic stromal-epithelial interactions in the mammary gland. J Mammary Gland Biol Neoplasia 15:301–318
45. Utani A, Nomizu M, Yamada Y (1997) Fibulin-2 binds to the short arms of laminin-5 and laminin-1 via conserved amino acid sequences. J Biol Chem 272:2814–2820
46. Klinowska TC, Soriano JV, Edwards GM, Oliver JM, Valentijn AJ et al (1999) Laminin and beta1 integrins are crucial for normal mammary gland development in the mouse. Dev Biol 215:13–32
47. Longmate WM, Monichan R, Chu ML, Tsuda T, Mahoney MG, et al. (2014) Reduced Fibulin-2 contributes to loss of basement membrane integrity and skin blistering in mice lacking integrin alpha3beta1 in the epidermis. J Invest Dermatol
48. Ono RN, Sengle G, Charbonneau NL, Carlberg V, Bachinger HP et al (2009) Latent transforming growth factor beta-binding proteins and fibulins compete for fibrillin-1 and exhibit exquisite specificities in binding sites. J Biol Chem 284:16872–16881
49. Miyazono K, Olofsson A, Colosetti P, Heldin CH (1991) A role of the latent TGF-beta 1-binding protein in the assembly and secretion of TGF-beta 1. EMBO J 10:1091–1101

50. Zhang H, Wu J, Dong H, Khan SA, Chu ML et al (2014) Fibulin-2 deficiency attenuates angiotensin II-induced cardiac hypertrophy by reducing transforming growth factor-beta signalling. Clin Sci (Lond) 126:275–288

51. Kouros-Mehr H, Werb Z (2006) Candidate regulators of mammary branching morphogenesis identified by genome-wide transcript analysis. Dev Dyn 235:3404–3412